Autoregressive Model of Channel Transfer Function for UWB Link inside a Passenger Car

Aniruddha Chandra, Pavel Kukolev, Tomáš Mikulášek, Aleš Prokeš

Department of Radio Electronics, Brno University of Technology, Brno 61600, Czech Republic.

E-Mail: aniruddha.chandra@ieee.org

Abstract—This article reports results of channel frequency transfer function measurements inside the passenger compartment of a four seated sedan car. The examined frequency range spans from 3 GHz to 11 GHz and covers the ultra wide band, a promising candidate for future automotive wireless standards. It is found that the complex transfer function may be decomposed into two terms, the first one being a real valued long term trend that characterizes frequency dependency with a power law, and the second term forms a complex correlative discrete series which may be represented via an autoregressive model. The proposed model is validated by comparing the simulated transfer function with the measured data. Simulated values for the coherence bandwidth, power delay profile, and the root mean square delay spread are also in good agreement with the experimental values.

Index Terms—AR model, UWB, transfer function, frequency dependency, intra-vehicle.

I. INTRODUCTION

A. Background

In the recent past, a number of ultra wide band (UWB) link measurements in passenger cars were being carried out [1]. Due to its large dynamic range, a vector network analyzer (VNA), is often preferred for such measurements. The two requirements for VNA based setups: transmitter (Tx) and the receiver (Rx) antennas should be within cable length, and the channel should be static, are also satisfied for in-car sounding experiments. A VNA provides channel transfer function (CTF) in the frequency domain, and proper characterization of the measured CTF is crucial for analysis of experimental data.

B. Contributions

- We propose an autoregressive (AR) process for channel frequency transfer function modelling of UWB links in car. To the best of our knowledge, this has not been attempted so far.
- We demonstrate that the AR process may be applied after removing the long term frequency trend from the transfer function. The method is different from earlier work on characterizing frequency dependency of intra-vehicular wireless channels, such as [2], where only simple models of large scale frequency variation was reported.

C. Organization

The next section provides description of the experimental setup and discusses the transfer function modelling in detail. The simulated transfer functions, following the model developed in Section 2, are validated against the measured data in Section 3. Finally, Section 4 concludes the paper and provides some directions for extending the work.

II. MEASUREMENT AND MODELLING

A. Experimental Setup

The measurements were performed inside a four seater passenger car, Skoda Octavia, parked in the basement garage. A 4 port VNA (Agilent E5071C) swept the entire UWB frequency range from 3 GHz to 11 GHz, with a frequency step of 10 MHz, creating a $N = (11-3) \times 10^9 / (10 \times 10^6) + 1 = 801$ point data set for each run. Port 1 and port 4 of the VNA were connected to the Tx and the Rx antennas, respectively, and the forward transmission coefficient, s_{41}, approximates the CTF, $H(f)$. A pair of identical conical monopole antennas were used as Tx and Rx, which were connected to the VNA through phase stable coaxial cables. The gain of a conical monopole antenna in the frequency range of interest (3-11 GHz) is almost constant [3]. Thus it is possible to analyze the measured CTF without considering antenna effects. The experimental setup and antenna positions inside the passenger compartment are shown in Fig. 1.

B. Long Term Variations

The magnitude of CTF has a overall downward slope with respect to frequency and the first step of our modelling involves separating this long term variation or trend, i.e. we express the complex CTF as

$$H(f) = \tilde{H}(f) \cdot |H(f)|_{\text{trend}} \qquad (1)$$

where $\tilde{H}(f)$ denotes the complex CTF after de-trending. The well known free space path loss formula suggests that the CTF is inversely proportional to frequency [4]. For real life wideband propagation a simple power law

$$|H(f)|_{\text{trend}} = K \cdot f^{-m} \qquad (2)$$

is generally used [5]. There also exists another exponential model [6]

$$20 \cdot \log_{10} |H(f)|_{\text{trend}} = K' \cdot \exp(-m'f) \qquad (3)$$

In Fig. 2 we depict a typical measured CTF and the corresponding trends with least mean square error fitting. The root mean square error for both the trends are comparable for the whole set of experimental data. However, we considered the power law given by (2) over the exponential one in (3) as
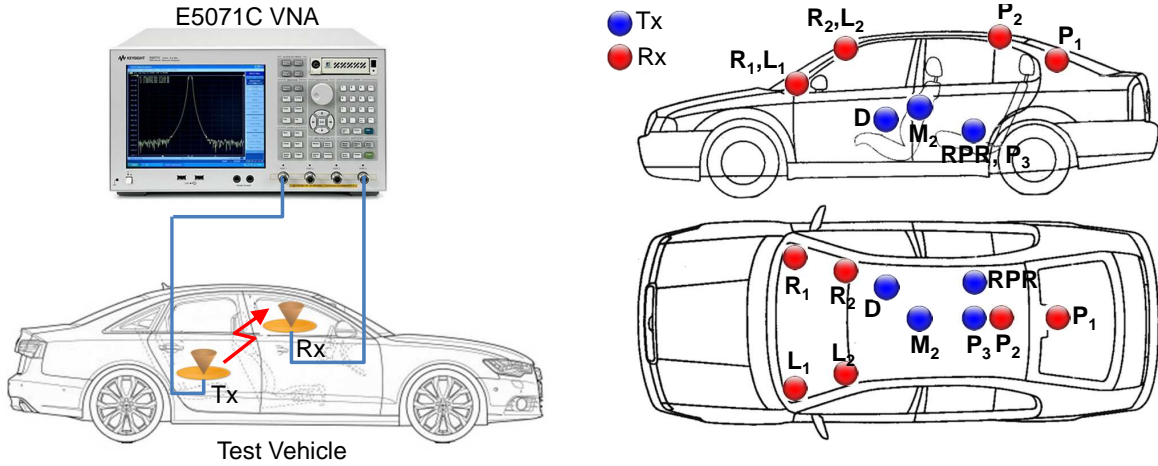
Fig. 1.   Measurement setup (left) and antenna placement inside car (right).
Tx legends - D: driver, RPR: rear passenger on right, P_3: middle of backseat, M_2: midpoint between two front seats.
Rx legends - L_1: left dashboard, R_1: right dashboard, L_2: left windshield, R_2: right windshield, P_1 and P_2: positions at rear part of the ceiling.
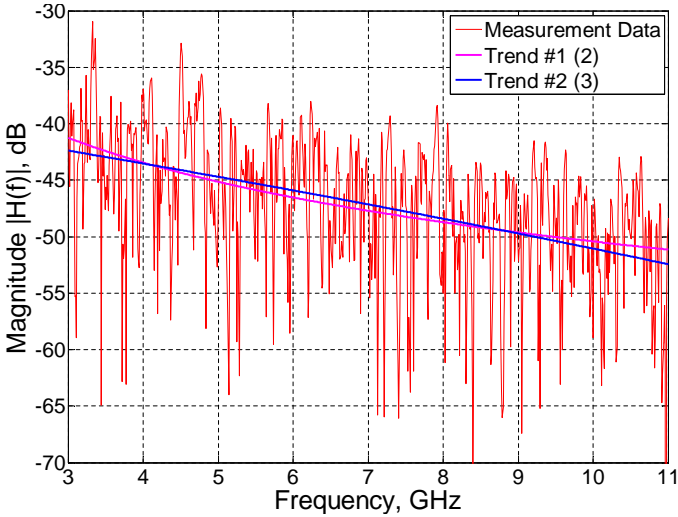
Fig. 2.   CTF and estimated trends (Tx position: P_3, Rx position: L_2).

TABLE I
PARAMETER VALUES OF THE FREQUENCY TREND FOR DIFFERENT TX AND
RX ANTENNA POSITIONS (MARKINGS ARE AS PER FIGURE 1).

Tx position	Rx position	Tx-Rx gap [m]	K [dB]	m	LoS/ nLoS
D	R_2	0.56	95.9481	0.6988	LoS
P_3	P_2	0.60	106.0515	0.7583	LoS
RPR	P_2	0.70	200.0803	1.2355	LoS
M_2	L_2	0.73	55.9457	0.4913	LoS
M_2	R_2	0.76	80.6947	0.6145	LoS
P_3	P_1	0.76	192.7777	1.1910	LoS
RPR	P_1	0.84	115.0652	0.8015	LoS
D	R_1	0.85	135.7254	0.9257	LoS
M_2	P_2	0.87	150.9870	0.9788	LoS
D	L_2	0.97	198.5332	1.2165	LoS
D	L_1	1.16	174.1665	1.1257	LoS
D	P_2	1.23	141.4975	0.9498	nLoS
P_3	L_2	1.23	125.0928	0.8776	nLoS
RPR	R_2	1.25	135.1506	0.9250	nLoS
P_3	R_2	1.28	178.1539	1.1457	nLoS
RPR	L_2	1.44	204.2820	1.2859	nLoS
D	P_1	1.48	62.0210	0.5556	nLoS
RPR	R_1	1.57	152.7682	1.0283	nLoS
P_3	L_1	1.62	148.1906	1.0062	nLoS
P_3	R_1	1.65	147.4560	1.0030	nLoS
RPR	L_1	1.74	157.8843	1.0637	nLoS

the former one is currently adopted in major UWB standards.
The parameters for different experiments are listed in Table I.

For indoor UWB propagation, a value range of $0.8 < m <$
1.4 was reported earlier [7]. The m values in Table I roughly
follows the limits. Our results are also consistent with previous
measurements inside car compartment [8] where a $1/f^2$ decay
was observed in the power spectra. The experiments conducted
at other parts (e.g. under the chasis) of the vehicle with less
favourable propagation modes results in a higher m [9].

C. AR Model for Short Term Variations

After finding out the long term trends, we proceed with the
characterization of the normalized CTF, namely, $\tilde{H}(f)$. The
variations of $\tilde{H}(f)$ resembles a correlated series, and for such a
series with low peaks and deep fades, an AR model is preferred
over moving average (MA) or hybrid ARMA models.

AR model for wideband indoor radio propagation was first
presented in [10], and later applied to UWB channel modelling

in [11] for indoor scenarios and in [12] for underground mines.
The normalized CTF under a q order AR process assumption
may be mathematically expressed as

$$\tilde{H}(f_n) - a_1\tilde{H}(f_{n-1}) - a_2\tilde{H}(f_{n-2}) \cdots - a_q\tilde{H}(f_{n-q}) = \xi_n \quad (4)$$

where, f_n; $n = 1, 2, \cdots N$, is the nth discrete frequency in
the CTF vector, a_k; $k = 1, 2, \cdots q$, are the complex AR
process coefficients, and ξ_n is the nth sample of a complex
Gaussian process with variance σ_ξ^2. A z-transform, $\tilde{H}(z) =$
$\sum_n \tilde{H}(f_n)z^{-n}$, allows us to view the CTF as the output of a
linear filter with transfer function, $\mathcal{G}(z) = \tilde{H}(z)/\xi(z)$, driven

by white Gaussian noise [10], i.e.

$$\mathcal{G}(z) = \frac{1}{1 - \sum_{k=1}^{q} a_k z^{-k}} = \prod_{k=1}^{q} \frac{1}{1 - p_k z^{-k}} \quad (5)$$

The poles of the filter, p_k; $k = 1, 2, \cdots q$, account for individual multipath clusters. Although a second order AR process was sufficient for indoor [11] and underground mines [12], we used a fifth order ($q = 5$) process as the car compartment exhibits multiple overlapped clusters. The poles (p_k) and the noise variance (σ_ξ^2) are found by solving the Yule-Walker equations in MATLAB. For finding initial conditions, we used a built in function `filtic()` with the first q entries of $\tilde{H}(f_n)$ and the AR model coefficients as arguments.

III. SIMULATION RESULTS AND DISCUSSIONS

A. Channel Transfer Function and Coherence BW

The CTF, $H(f)$, is obtained through combining the long term frequency dependence using parameters from Table I with the simulated short term AR model based variations. The measured and simulated transfer functions for one particular Tx-Rx pair is shown in Fig. 3.
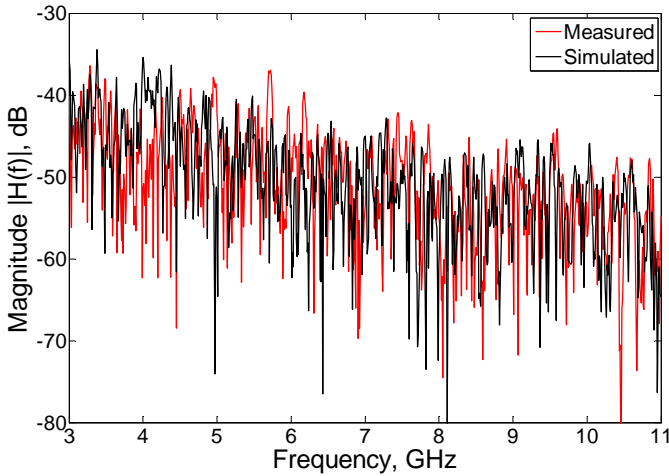
Fig. 3. Measured and simulated CTF (Tx position: RPR, Rx position: L_1).

The frequency autocorrelation function (ACF), $R(\Delta f)$, may be found from the channel transfer function as [13]

$$R(\Delta f) = \int_{-\infty}^{\infty} H(f) H^*(f + \Delta f) \, \mathrm{d}f \quad (6)$$

which provides a measure of the frequency selectivity. The range between DC or zero frequency, where normalized ACF attains its peak value of unity, and the frequency where ACF falls to 50% of or 3 dB lower than its peak value, is defined as the coherence bandwidth (BW), B_C. From Fig. 4, it can be seen that the measured and simulated transfer functions manifest almost similar B_C values.

A channel is considered *flat* in the coherence BW interval, i.e. if two different frequencies are separated by more than B_C, the channel exhibits uncorrelated fading at these two frequencies. There is a more direct method available for calculation
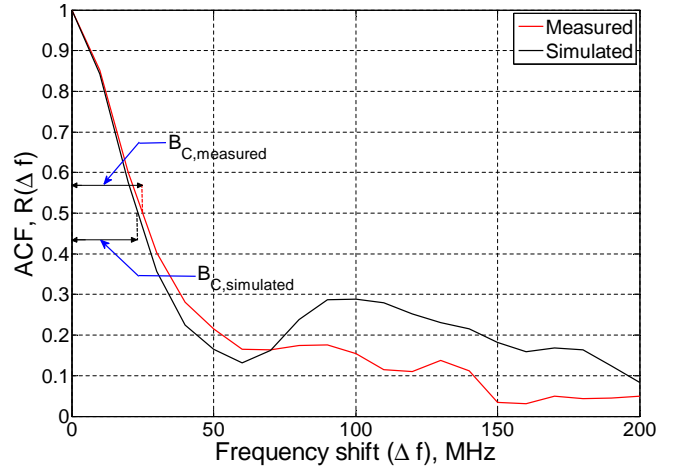
Fig. 4. Comparison of frequency ACF (Tx position: P_3, Rx position: R_2).

of coherence BW [14]. However, we computed B_C via the classical approach as the BW spans over only few samples for the current frequency step size (10 MHz), and there might be large approximation errors involved in the direct method.

B. PDP and RMS Delay Spread

Next, the complex channel impulse responses (CIRs), $h(t) = \mathcal{F}^{-1} H(f)$, are obtained through inverse fast Fourier transform (IFFT) method. Power delay profile (PDP) is closely related with the CIR, $\mathrm{PDP}(t) = |h(t)|^2$, and describes the variation of the average received power in dBm (when the transmit power of VNA is set to 0 dBm) as a function of delay time [15]. Fig. 5 shows the comparison of the measured PDP with the simulated PDP, and one can find that there is a close match.
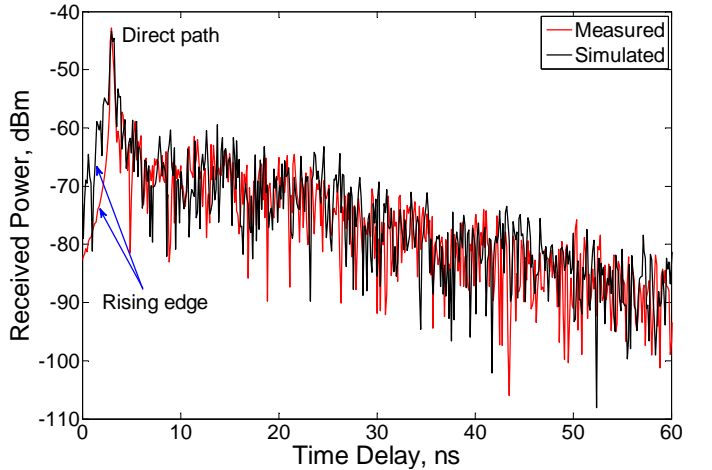
Fig. 5. Measured and simulated PDPs (Tx position: P_3, Rx position: P_1).

A quantitative comparison between the measured PDP and the simulated PDP can be performed by noting the similarity of the root mean square (RMS) delay spreads obtained for both the delay profiles. RMS delay spread is the second central

moment of the PDP

$$\tau_{\mathrm{rms}} = \sqrt{\int_0^{\tau_{\max}} (t - \bar{\tau})^2 \cdot \mathrm{PDP}_n(t)\, \mathrm{d}t} \qquad (7)$$

where $\tau_{\max}$ denotes the maximum excess delay, $\mathrm{PDP}_n(t) = \mathrm{PDP}(t)/\int_0^{\tau_{\max}} \mathrm{PDP}(t)\mathrm{d}t$ is normalized PDP, and $\bar{\tau} = \int_0^{\tau_{\max}} t \cdot \mathrm{PDP}_n(t)\mathrm{d}t$ is the mean excess delay.

For calculating the RMS delays, the rising edge of the PDP is cut off and the time origin is shifted to the time index that corresponds to the peak. This time shifting helps in rendering the delays as excess delays relative to the peak or first arriving path which has a zero delay. Although the rising edge may be suppressed with appropriate windowing (Hamming, Hann, Blackman etc.) during the IFFT post-processing, the process is avoided here. Further, only those multipath components (MPCs) having a delay less than $\tau_{\max} = 60$ ns are considered. This step ensures that the truncated PDP does not hit the noise floor. According to the Agilent E5071C VNA data sheet, the noise floor is -120 dBm/Hz. Hence, for a 10Hz IF bandwidth, it is good enough to consider MPCs upto -110 dBm. Finally, the PDPs are normalized so that the peak occurs at 0 dB. The measured RMS delay values are between 5 to 10 ns, and are consistent with time domain measurements of intra-vehicle UWB links [16].

The comparison of RMS delay spreads reveals that the simulated PDP matches closely with the measured PDP as the percentage of error

$$\% \text{ error} = \frac{\tau_{\mathrm{rms,simulated}} - \tau_{\mathrm{rms,measured}}}{\tau_{\mathrm{rms,measured}}} * 100 \qquad (8)$$

is typically 10%, with values ranging between 2% to 30%. It is also interesting to note that the error is always positive, i.e. the simulated PDP slightly overestimates τ_{rms}.

IV. CONCLUSIONS AND FUTURE WORK

The key finding of the paper is, the transfer function of a intra-vehicle UWB channel can be modelled with an AR process after removing the frequency dependent trend. Simulated transfer functions using the AR process parameters and the trend parameters exhibit close match with the measured values. The similarity of coherence BW, PDP, and RMS delay spreads further validates the model.

The next step is to study the dependence of the parameters for the AR process and the long term trends on frequency and Tx-Rx separation. This would lead to development of a comprehensive model for intra-car communication which can predict transfer function for arbitrary Tx/ Rx placement with a certain degree of accuracy. It would be also interesting to investigate whether this model can be extended to intra-car millimeter wave links.

REFERENCES

[1] I. G. Zuazola, J. M. Elmirghani, and J. C. Batchelor, "High-speed ultra-wide band in-car wireless channel measurements," *IET communications*, vol. 3, no. 7, pp. 1115–23, Jul. 2009.

[2] M. Schack, J. Jemai, R. Piesiewicz, R. Geise, I. Schmidt, and T. Kürner, "Measurements and analysis of an in-car UWB channel," in *IEEE Vehicular Technology Conference (VTC 2008-Spring)*, Singapore, May 2008, pp. 459–63.

[3] J. S. McLean, R. Sutton, A. Medina, H. Foltz, and J. Li, "The experimental characterization of uwb antennas via frequency-domain measurements," *IEEE Antennas and Propagation Magazine*, vol. 49, no. 6, pp. 192–202, Dec. 2007.

[4] W. Q. Malik, D. J. Edwards, and C. J. Stevens, "Frequency-dependent pathloss in the ultrawideband indoor channel," in *IEEE International Conference on Communications (ICC)*, vol. 12, Istanbul, Turkey, Jun. 2006, pp. 5546–51.

[5] J. Kunisch and J. Pamp, "Measurement results and modeling aspects for the UWB radio channel," in *IEEE Conference on Ultra Wideband Systems and Technologies (UWBST)*, vol. 1, Baltimore, MD, USA, May 2002, pp. 19–23.

[6] A. Álvarez, G. Valera, M. Lobeira, R. P. Torres, and J. L. C. García, "New channel impulse response model for UWB indoor system simulations," in *IEEE Vehicular Technology Conference (VTC 2003-Spring)*, vol. 1, Jeju, Korea, Apr. 2003, pp. 1–5.

[7] C. C. Chong, Y. E. Kim, S. K. Yong, and S. S. Lee, "Statistical characterization of the UWB propagation channel in indoor residential environment," *Wireless Communications and Mobile Computing*, vol. 5, no. 5, pp. 503–12, Aug. 2005.

[8] T. Kobayashi, "Measurements and characterization of ultra wideband propagation channels in a passenger-car compartment," in *IEEE International Symposium on Spread Spectrum Techniques and Applications*, Manaus, Amazon, Brazil, Aug. 2006, pp. 228–32.

[9] C. U. Bas and S. C. Ergen, "Ultra-wideband channel model for intra-vehicular wireless sensor networks beneath the chassis: from statistical model to simulations," *IEEE Transactions on Vehicular Technology*, vol. 62, no. 1, pp. 14–25, Jan. 2013.

[10] S. J. Howard and K. Pahlavan, "Autoregressive modeling of wideband indoor radio propagation," *IEEE Transactions on Communications*, vol. 40, no. 9, pp. 1540–52, Sep. 1992.

[11] S. S. Ghassemzadeh, R. Jana, C. W. Rice, W. Turin, and V. Tarokh, "Measurement and modeling of an ultra-wide bandwidth indoor channel," *IEEE Transactions on Communications*, vol. 52, no. 10, pp. 1786–96, Oct. 2004.

[12] A. Chehri and P. Fortier, "Frequency domain analysis of UWB channel propagation in underground mines," in *IEEE Vehicular Technology Conference (VTC 2006-Fall)*, Montreal, Quebec, Canada, Sep. 2006, pp. 1–5.

[13] I. Cuiñas and M. G. Sánchez, "Measuring, modeling, and characterizing of indoor radio channel at 5.8 GHz," *IEEE Transactions on Vehicular Technology*, vol. 50, no. 2, pp. 526–35, Mar. 2001.

[14] M. Ghaddar, L. Talbi, and G. Y. Delisle, "Coherence bandwidth measurement in indoor broadband propagation channel at unlicensed 60 GHz band," *Electronics Letters*, vol. 48, no. 13, pp. 795–97, Jun. 2012.

[15] G. J. M. Janssen, P. A. Stigter, and R. Prasad, "Wideband indoor channel measurements and BER analysis of frequency selective multipath channels at 2.4, 4.75, and 11.5 GHz," *IEEE Transactions on Communications*, vol. 44, no. 10, pp. 1272–88, Oct. 1996.

[16] A. Chandra, J. Blumenstein, T. Mikulásek, J. Vychodil, M. Pospísil, R. Maršálek, A. Prokeš, T. Zemen, and C. Mecklenbräuker, "CLEAN algorithms for intra-vehicular time-domain UWB channel sounding," in *International Conference on Pervasive and Embedded Computing and Communication Systems (PECCS)*, Angers, France, Feb. 2015, pp. 224–29.